Quantum repeaters using a heralded scheme with remote swapping and two-photon interference

Yi Zhong(钟艺)[1,2,*] Chang Li(李畅)[1,2,3], and Hui Yan(颜辉)[1,2]

[1]Key Laboratory of Atomic and Subatomic Structure and Quantum Control (Ministry of Education), Guangdong Basic Research Center of Excellence for Structure and Fundamental Interactions of Matter, and School of Physics, South China Normal University, Guangzhou 510006, China

[2]Guangdong Provincial Key Laboratory of Quantum Engineering and Quantum Materials, Guangdong-Hong Kong Joint Laboratory of Quantum Matter, and Frontier Research Institute for Physics, South China Normal University, Guangzhou 510006, China

[3]Quantum Science Center of Guangdong-Hong Kong-Macao Greater Bay Area, Shenzhen, China

(October 12, 2026)

Efficient long-distance entanglement distribution is a key requirement for a global quantum internet. Quantum repeaters overcome photon loss in optical fibers, offering a route to long-distance entanglement distribution. Here, we study heralded quantum repeater architectures that are based on two-photon interference and integrate local or remote swapping. We derive an analytical expression for the entanglement distribution time as a function of transmission distance for both heralded local-swapping and remote-swapping schemes. This expression provides physical insight into how repeaters overcome channel loss in long-haul fibers. Considering a realistic quantum memory, we present theoretical curves showing the effect of finite memory lifetime on the entanglement distribution time. By comparing optimal distribution times over distances up to thousands of kilometers, we determine the optimal nesting architectures for the single-repeater channel in each scheme and compare the optimal distribution rates and entanglement fidelities of these schemes at various distances. Finally, by examining the limiting cases of zero channel loss, zero device loss, and lossless repeater systems, we find fundamental performance bounds for quantum repeaters. These results provide practical design principles for scalable quantum repeater networks and pave the way toward continent-scale quantum communication.

Keywords: heralded repeater scheme, remote swapping, two-photon interference, optimal nesting architecture
PACS: 03.67.Hk, 03.67.Bg, 03.67.-a
DOI:
CSTR:

1. Introduction

The quantum internet interconnects quantum information processors via quantum communication. [1–4] A central task is the distribution of entanglement between remote nodes, which underpins distributed quantum computing, [5–8] quantum sensor networks, [9–12] and global-scale quantum communication. [13–16] Photons serve as natural flying qubits for long-distance transmission, enabling entanglement between distant stationary qubits. [17–25] However, photonic signals suffer from exponential attenuation in optical fibers, which fundamentally limits the achievable distance for direct entanglement distribution. To overcome this challenge, quantum repeaters have been proposed to mitigate photon loss in quantum communication channels. [26,27] By dividing a long channel into shorter segments, quantum repeaters first establish independent entangled states in each segment and then perform nested entanglement swapping to extend the entanglement distance. Consequently, quantum repeaters represent a promising approach for long-distance entanglement distribution.

*Corresponding author. E-mail: yizhong369575@163.com

The Briegel-Dür-Cirac-Zoller (BDCZ) scheme proposes combining segmented entanglement establishment with nested local swapping for long-distance entanglement distribution. [26] The Duan-Lukin-Cirac-Zoller (DLCZ) scheme provides a seminal framework based on atomic ensembles and linear optics, designed for a specific experimental implementation. [27] Over the past two decades, all key components of the DLCZ scheme have been experimentally realized, [28–30] with further advances including multiplexing-enhanced quantum memories, [31–36] telecom-wavelength photon interfaces, [17–20,22–25] the post-selected scheme with local swapping, [37] and heralded entanglement swapping. [38,39] These developments have laid the foundation for large-scale repeater networks. To date, a complete theoretical framework for calculating the entanglement distribution time has been established for the post-selected scheme with local swapping. [37] However, it remains an open question how to calculate the distribution time for heralded schemes with remote or local swapping. Furthermore, optimizing the nested architecture of a quantum repeater channel to minimize the distribution time is an important open issue requiring further investigation.

In this work, we calculate the entanglement distribution time for quantum repeater schemes that are based on two-photon interference and that combine local or remote swapping with a heralded scheme. Specifically, we derive a theoretical formula that explicitly relates the distribution time to the transmission distance; this formula serves as the key analytical tool for our subsequent analysis. Guided by the physical insight provided by this formula, we analyze the underlying mechanism by which quantum repeaters overcome channel loss in long-distance fiber transmission. Considering a realistic quantum memory, we present theoretical curves showing the effect of finite memory lifetime on the entanglement distribution time. By comparing the optimal distribution times over distances up to thousands of kilometers, we identify the optimal nesting architectures for the single-repeater channel in each scheme. When mode multiplexing is considered, we compare the optimal distribution rates of the heralded schemes and the post-selected scheme at various distances. Under realistic device efficiencies, the heralded scheme with remote swapping always yields a larger distribution rate than either the heralded scheme with local swapping or the post-selected scheme with local swapping. Furthermore, by comparing the entanglement fidelity of these schemes, we find that remote swapping can mitigate the decline in fidelity with distance more effectively than local swapping under the same nested architecture. Finally, we extend our theoretical analysis to extreme parameter regimes, including the limiting cases of zero channel loss, zero device loss, and lossless repeater systems. These results provide design guidelines for large-scale quantum repeater networks.

The paper is organized as follows. In Sec. 2, we introduce two quantum repeater schemes based on two-photon interference, each of which combines local or remote swapping with a heralded scheme. In Sec. 3, we calculate the entanglement distribution time for these schemes and derive theoretical formulas that relate the distribution time to the transmission distance. We also define ratio functions that provide an intuitive explanation of the physical mechanism by which quantum repeaters overcome fiber channel loss. In Sec. 4, we analyze in detail how quantum repeaters mitigate channel loss over long distances, using plots of distribution time as a function of distance (derived from the theoretical formula) together with ratio functions. Furthermore, we present theoretical curves showing the effect of finite memory lifetime on the entanglement distribution time when a realistic quantum memory is considered. In Sec. 5, we identify the optimal nesting architectures for the single-repeater channel in each scheme by comparing the optimal distribution times over distances up to thousands of kilometers. In addition, we compare the optimal distribution rates and entanglement fidelities of these schemes. In Sec. 6, we find fundamental performance bounds for quantum repeaters in extreme parameter regimes, such as zero channel loss, zero device loss, and lossless repeater systems. Finally, Sec. 7 summarizes our findings and outlines prospects for future work. The theoretical details and supplementary information are provided in the Appendices.

2. Schemes of quantum repeaters

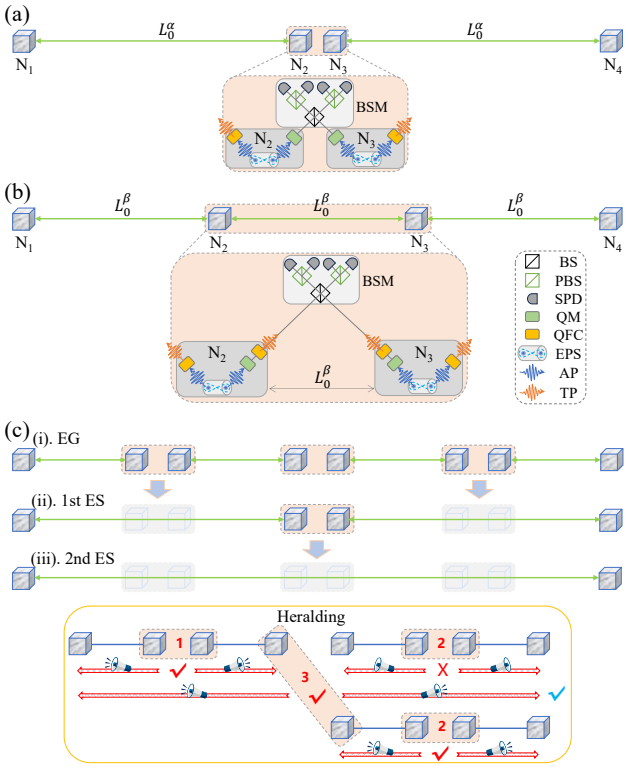


Fig. 1. Schemes of quantum repeaters. (a) Local swapping. For entanglement swapping between nodes N_2 and N_3, blue photons stored in the QMs are simultaneously read out and subjected to a BSM. (b) Remote swapping. The swapping operation between nodes N_2 and N_3 is remotely implemented with a distance L_0^β. Blue photons are converted via QFCs to the orange photons at telecom wavelength, and then transmitted through fibers to a BSM. (c) Quantum repeater with heralded scheme. (i)-(iii) denote the entanglement generation (EG), the first entanglement swapping (1st ES), and the second entanglement swapping (2nd ES) for a nested quantum repeater. For the heralded scheme, when swapping (2) fails, swapping (1) does not need to be recreated. Swapping (3) can be completed only after swapping (2) is successfully regenerated (cyan $\surd$). Red $\surd$ or X denotes success or failure of the swapping operation. Cyan $\surd$ or X represents success or failure for entanglement distribution. BSM: Bell-state measurement. PBS: Polarization beam splitter. BS: Beam splitter. SPD: Single-photon detector. QM: Quantum memory. QFC: Quantum frequency converter. EPS: Entangled photon source. AP: Photon in the atomic operating band. TP: Telecom-wavelength photon.

In a quantum repeater architecture, a communication channel is divided into segments by intermediate nodes. Entanglement is first generated within each segment and subse-

quently extended over long distances via sequential entanglement swapping. [26,27] In Fig. 1(a), we present a realistic repeater scheme based on two-photon interference, denoted as local swapping. For a nesting level σ, the total channel length L is divided into 2^σ segments, each of length $L_0^\alpha = L/2^\sigma$. Telecom-wavelength photons are widely employed for long-distance entanglement distribution. Motivated by this consideration, we introduce a modified repeater architecture incorporating remote entanglement swapping, as shown in Fig. 1(b) and denoted as remote swapping. In this case, the channel is divided into $2^{\sigma+1}-1$ segments with length $L_0^\beta = L/(2^{\sigma+1}-1)$, where the distance required for remote entanglement swapping is assumed to be equal to the elementary link length. As a result, for a given nesting level σ and total channel length L, remote swapping achieves finer segmentation than local swapping.

The extension of entanglement relies on sequential entanglement swapping, where each successful swapping operation doubles the entanglement distance for local swapping [Fig. 1(c)]. In the conventional approach, BSMs at entanglement swapping are performed only after entanglement has been successfully established in all segments. [31,32,37,40,41] A failure in any BSM results in the failure of the entire distribution process. However, success can be verified a posteriori, for example via Bell inequality tests. [37] Thus, this approach is referred to as the post-selected scheme. Alternatively, BSM outcomes can be used to herald successful entanglement swapping in real time. As illustrated in the inset of Fig. 1(c), in this heralded scheme, a failed swapping operation affects only the corresponding segment, while previously established entanglement links are preserved. The failed segment can then be regenerated without restarting the entire protocol, enabling more efficient entanglement distribution.

Combining this heralded scheme with local swapping and with remote swapping yields two quantum repeater schemes based on two-photon interference. For both heralded schemes, with local or remote swapping, long-distance entanglement distribution can be achieved by using a BSM scheme that projects onto the orthogonal-polarization Bell state, i.e., the state $1/\sqrt{2}(|H\rangle_1|V\rangle_n + |V\rangle_1|H\rangle_n)$, where n labels the quantum node. The scheme for long-distance distribution of polarization entanglement is discussed in detail in Appendix A.

3. Theoretical model of quantum repeater

For the heralded scheme with local swapping, when entanglement is successfully established in an elementary link (e.g., including two nodes), the time required for entanglement creation is given by [42]

$$T_0^{\alpha H} = \frac{L_0^\alpha}{c_0}\frac{1}{P_0^{\alpha H}}, \tag{1}$$

where $P_0^{\alpha H} = (p_{eD})^2(\eta_c)^2(\eta_{tR}^\alpha)^2\eta_{\rm BSM}(\eta_d)^2$ is the success probability for entanglement creation in an elementary link. Here, p_{eD} denotes the generation probability of entangled photon pairs. The fiber transmittance for local swapping is given by $\eta_{tR}^\alpha = 10^{-(\alpha_{\rm fiber}\times 0.5 L_0^\alpha)/10}$, where $\alpha_{\rm fiber}$ is the fiber attenuation coefficient. Furthermore, η_c, η_d, and $\eta_{\rm BSM}$ represent the conversion efficiency of QFC, the detection efficiency of SPD, and the heralding efficiency of BSM, respectively. The factor L_0^α/c_0 corresponds to the classical communication time over one elementary link of length L_0^α. Upon successful creation, the elementary link produces an entangled state that is either $|H\rangle_n|V\rangle_{n+1}$ or $|V\rangle_n|H\rangle_{n+1}$, with the subscript n labeling the quantum nodes.

We now consider the entanglement distribution time for $\sigma = 1$, which includes elementary links 1 and 2. When both elementary links 1 and 2 succeed, each with probability $P_0^{\alpha H}$, the waiting time for both to succeed is $T_0^{\alpha H}\nu_0^{\alpha H}P_0^{\alpha H}$, where $\nu_0^{\alpha H} = \frac{1}{P_0^{\alpha H}}\frac{3-2P_0^{\alpha H}}{2-P_0^{\alpha H}}$ is the average number of tries for both elementary links 1 and 2 to succeed. This derivation is presented in Appendix B. Thus, upon successful creation, there are 2^2 possible combinations of the resulting entangled states: ($|H_1, V_2\rangle$, $|H_3, V_4\rangle$), ($|V_1, H_2\rangle$, $|V_3, H_4\rangle$), ($|H_1, V_2\rangle$, $|V_3, H_4\rangle$), and ($|V_1, H_2\rangle$, $|H_3, V_4\rangle$). Among these, two combinations, ($|H_1, V_2\rangle$, $|H_3, V_4\rangle$) and ($|V_1, H_2\rangle$, $|V_3, H_4\rangle$), are compatible with the first heralded entanglement swapping. Conditioned on elementary links 1 and 2 having established entangled states that satisfy the requirements for the first heralded entanglement swapping, the accumulated waiting time becomes $T_0^{\alpha H}\nu_0^{\alpha H}P_0^{\alpha H}\times 2$. Here, the factor 2 denotes the reciprocal of the probability of satisfying the first heralded entanglement swapping. After completion of the first heralded entanglement swapping, the total time for a successful distribution is

$$T_1^{\alpha H} = \frac{L_0^\alpha}{c_0}\frac{1}{P_0^{\alpha H}}\frac{3-2P_0^{\alpha H}}{2-P_0^{\alpha H}}\times 2 + \frac{2}{2}\frac{L_0^\alpha}{c_0}\frac{1}{P_1^{\alpha H}}. \tag{2}$$

Here, $P_1^{\alpha H} = \eta_{\rm BSM}^\alpha/\eta_1^{\alpha H}$ is the success probability of the first heralded entanglement swapping, with $\eta_1^{\alpha H} = 1/(2-\eta_{\rm BSM}^\alpha)$ [37]. Here, $\eta_{\rm BSM}^\alpha = (\eta_m)^2\eta_{\rm BSM}(\eta_d)^2$ is the overall BSM efficiency at entanglement swapping for local swapping. η_m is the storage efficiency of QM. The term $(2/2)(L_0^\alpha/c_0)$ corre-

sponds to the classical communication time for heralding entangled states at $\sigma = 1$.

We now consider the case of $\sigma = 2$. When all four elementary links (1-4) succeed, each with probability $P_0^{\alpha H}$, the waiting time for all four to succeed is given by $\frac{L_0^\alpha}{c_0}\frac{1}{P_0^{\alpha H}}\frac{3-2P_0^{\alpha H}}{2-P_0^{\alpha H}}\frac{3-2(P_0^{\alpha H})^2}{2-(P_0^{\alpha H})^2}$. This derivation is presented in Appendix B. There are 2^4 possible combinations of entangled states. Among these, 2^2 combinations, namely ($|H_1, V_2\rangle$, $|H_3, V_4\rangle$), ($|V_1, H_2\rangle$, $|V_3, H_4\rangle$), ($|H_5, V_6\rangle$, $|H_7, V_8\rangle$), and ($|V_5, H_6\rangle$, $|V_7, H_8\rangle$), are compatible with the first heralded entanglement swapping. Consequently, the accumulated waiting time becomes $\frac{L_0^\alpha}{c_0}\frac{1}{P_0^{\alpha H}}\frac{3-2P_0^{\alpha H}}{2-P_0^{\alpha H}}\frac{3-2(P_0^{\alpha H})^2}{2-(P_0^{\alpha H})^2} \times 2^2$ once the elementary links have established entangled states that satisfy the requirements for the first heralded entanglement swapping. Here, the factor 2^2 denotes the reciprocal of the probability of satisfying the first heralded entanglement swapping. Once the two $\sigma = 1$ links are completed, there are 2^2 possible combinations of entangled states: ($|H_1, V_2, H_3, V_4\rangle$, $|H_5, V_6, H_7, V_8\rangle$), ($|V_1, H_2, V_3, H_4\rangle$, $|V_5, H_6, V_7, H_8\rangle$), ($|H_1, V_2, H_3, V_4\rangle$, $|V_5, H_6, V_7, H_8\rangle$), and ($|V_1, H_2, V_3, H_4\rangle$, $|H_5, V_6, H_7, V_8\rangle$). Among these, two combinations, namely ($|H_1, V_2, H_3, V_4\rangle$, $|H_5, V_6, H_7, V_8\rangle$) and ($|V_1, H_2, V_3, H_4\rangle$, $|V_5, H_6, V_7, H_8\rangle$), are compatible with the second heralded entanglement swapping. Hence, once the $\sigma = 1$ links have established entangled states that satisfy the requirements for the second heralded entanglement swapping, the accumulated waiting time becomes $\frac{L_0^\alpha}{c_0}\frac{1}{P_0^{\alpha H}}\frac{3-2P_0^{\alpha H}}{2-P_0^{\alpha H}}\frac{3-2(P_0^{\alpha H})^2}{2-(P_0^{\alpha H})^2} \times 2^2 + \frac{L_0^\alpha}{c_0}\frac{1}{P_1^{\alpha H}}\frac{3-2P_1^{\alpha H}}{2-P_1^{\alpha H}} \times 2$. Here, the factor 2 is the reciprocal of the probability that the entangled states are compatible with the second heralded entanglement swapping. Thus, after completion of the second heralded entanglement swapping, the total entanglement distribution time is

$$\begin{aligned} T_2^{\alpha H} = {} & \frac{L_0^\alpha}{c_0}\frac{1}{P_0^{\alpha H}}\frac{3-2P_0^{\alpha H}}{2-P_0^{\alpha H}}\frac{3-2(P_0^{\alpha H})^2}{2-(P_0^{\alpha H})^2} \times 2^2 \\ & + \frac{2}{2}\frac{L_0^\alpha}{c_0}\frac{1}{P_1^{\alpha H}}\frac{3-2P_1^{\alpha H}}{2-P_1^{\alpha H}} \times 2 + \frac{4}{2}\frac{L_0^\alpha}{c_0}\frac{1}{P_2^{\alpha H}}, \end{aligned} \tag{3}$$

where $P_2^{\alpha H} = \eta_{\mathrm{BSM}}^\alpha (\eta_1^{\alpha H})^2 / \eta_2^{\alpha H}$ is the success probability of the second heralded entanglement swapping, with $\eta_2^{\alpha H} = \eta_1^{\alpha H}/(2 - \eta_1^{\alpha H}\eta_{\mathrm{BSM}}^\alpha)$. [37] The term $(4/2)(L_0^\alpha/c_0)$ corresponds to the classical communication time for heralding entangled states at $\sigma = 2$.

We now extend the analysis to higher nesting levels. For $\sigma = 3$, when all eight elementary links (1-8) succeed, each with probability $P_0^{\alpha H}$, the waiting time for all eight to succeed is given by $\frac{L_0^\alpha}{c_0}\frac{1}{P_0^{\alpha H}}\frac{3-2P_0^{\alpha H}}{2-P_0^{\alpha H}}\frac{3-2(P_0^{\alpha H})^2}{2-(P_0^{\alpha H})^2}\frac{3-2(P_0^{\alpha H})^4}{2-(P_0^{\alpha H})^4}$. There are 2^8 possible combinations of entangled states. Among these, 2^3 combinations are compatible with the first heralded entanglement swapping. Among the 2^3 compatible combinations at the first level, 2^2 combinations are compatible with the second heralded entanglement swapping. Finally, among the 2^2 compatible combinations at the second level, two combinations are compatible with the third heralded entanglement swapping. Thus, after completion of the third heralded entanglement swapping, the total entanglement distribution time is

$$\begin{aligned} T_3^{\alpha H} = {} & \frac{L_0^\alpha}{c_0}\frac{1}{P_0^{\alpha H}}\frac{3-2P_0^{\alpha H}}{2-P_0^{\alpha H}}\frac{3-2(P_0^{\alpha H})^2}{2-(P_0^{\alpha H})^2} \\ & \times \frac{3-2(P_0^{\alpha H})^4}{2-(P_0^{\alpha H})^4} \times 2^5 + \frac{2}{2}\frac{L_0^\alpha}{c_0}\frac{1}{P_1^{\alpha H}}\frac{3-2P_1^{\alpha H}}{2-P_1^{\alpha H}} \\ & \times \frac{3-2(P_1^{\alpha H})^2}{2-(P_1^{\alpha H})^2} \times 2 + \frac{4}{2}\frac{L_0^\alpha}{c_0}\frac{1}{P_2^{\alpha H}}\frac{3-2P_2^{\alpha H}}{2-P_2^{\alpha H}} \\ & \times 2 + \frac{8}{2}\frac{L_0^\alpha}{c_0}\frac{1}{P_3^{\alpha H}}, \end{aligned} \tag{4}$$

where $P_3^{\alpha H} = \eta_{\mathrm{BSM}}^\alpha (\eta_2^{\alpha H})^2 / \eta_3^{\alpha H}$ is the success probability of the third heralded entanglement swapping, and $\eta_3^{\alpha H} = \eta_2^{\alpha H}/(2 - \eta_2^{\alpha H}\eta_{\mathrm{BSM}}^\alpha)$. [37] The term $(8/2)(L_0^\alpha/c_0)$ corresponds to the classical communication time for heralding entangled states at $\sigma = 3$.

For $\sigma = 4$, when all sixteen elementary links (1-16) succeed, each with probability $P_0^{\alpha H}$, the waiting time for all sixteen to succeed is given by $\frac{L_0^\alpha}{c_0}\frac{1}{P_0^{\alpha H}}\frac{3-2P_0^{\alpha H}}{2-P_0^{\alpha H}}\frac{3-2(P_0^{\alpha H})^2}{2-(P_0^{\alpha H})^2}\frac{3-2(P_0^{\alpha H})^4}{2-(P_0^{\alpha H})^4}\frac{3-2(P_0^{\alpha H})^8}{2-(P_0^{\alpha H})^8}$. There are 2^{16} possible combinations of entangled states. Among these, 2^4 combinations are compatible with the first heralded entanglement swapping. Among the 2^4 compatible combinations, 2^3 are compatible with the second heralded entanglement swapping. Among these 2^3 combinations, 2^2 are compatible with the third heralded entanglement swapping. Finally, among these 2^2 combinations, two are compatible with the fourth heralded entanglement swapping. Thus, when the fourth heralded entanglement swapping is completed, the total

time is given by

$$
\begin{aligned}
T_4^{\alpha H} = & \frac{L_0^\alpha}{c_0}\frac{1}{P_0^{\alpha H}}\frac{3-2P_0^{\alpha H}}{2-P_0^{\alpha H}}\frac{3-2(P_0^{\alpha H})^2}{2-(P_0^{\alpha H})^2} \\
& \times \frac{3-2(P_0^{\alpha H})^4}{2-(P_0^{\alpha H})^4}\frac{3-2(P_0^{\alpha H})^8}{2-(P_0^{\alpha H})^8} \times 2^{12} + \frac{2}{2}\frac{L_0^\alpha}{c_0} \\
& \times \frac{1}{P_1^{\alpha H}}\frac{3-2P_1^{\alpha H}}{2-P_1^{\alpha H}}\frac{3-2(P_1^{\alpha H})^2}{2-(P_1^{\alpha H})^2}\frac{3-2(P_1^{\alpha H})^4}{2-(P_1^{\alpha H})^4} \\
& \times 2 + \frac{4}{2}\frac{L_0^\alpha}{c_0}\frac{1}{P_2^{\alpha H}}\frac{3-2P_2^{\alpha H}}{2-P_2^{\alpha H}}\frac{3-2(P_2^{\alpha H})^2}{2-(P_2^{\alpha H})^2} \times 2 \\
& + \frac{8}{2}\frac{L_0^\alpha}{c_0}\frac{1}{P_3^{\alpha H}}\frac{3-2P_3^{\alpha H}}{2-P_3^{\alpha H}} \times 2 + \frac{16}{2}\frac{L_0^\alpha}{c_0}\frac{1}{P_4^{\alpha H}},
\end{aligned}
\tag{5}
$$

where $P_4^{\alpha H} = \eta_{\rm BSM}^{\alpha}(\eta_3^{\alpha H})^2/\eta_4^{\alpha H}$ is the success probability of the fourth heralded entanglement swapping, and $\eta_4^{\alpha H} = \eta_3^{\alpha H}/(2-\eta_3^{\alpha H}\eta_{\rm BSM}^{\alpha})$. [37] The term $(16/2)(L_0^\alpha/c_0)$ corresponds to the classical communication time for heralding entangled states at $\sigma = 4$. Generalizing to arbitrary σ, after completing the σ-level heralded entanglement swapping, the entanglement distribution time can be expressed as

$$
\begin{aligned}
T_\sigma^{\alpha H} &= T_{0\sigma}^{\alpha H} + T_{i\sigma}^{\alpha H} + T_{L\sigma}^{\alpha H} \\
&= 2^{(2^\sigma-\sigma)}\frac{L_0^\alpha}{c_0}\frac{1}{P_0^{\alpha H}}\prod_1^\sigma\frac{3-2(P_0^{\alpha H})^{2^{\sigma-1}}}{2-(P_0^{\alpha H})^{2^{\sigma-1}}} \\
&\quad + 2\times\sum_i^\sigma\left(\frac{2^{i-1}}{2}\frac{L_0^\alpha}{c_0}\frac{1}{P_{i-1}^{\alpha H}}\prod_i^\sigma\frac{3-2(P_{i-1}^{\alpha H})^{2^{\sigma-i}}}{2-(P_{i-1}^{\alpha H})^{2^{\sigma-i}}}\right) \\
&\quad + \frac{2^\sigma}{2}\frac{L_0^\alpha}{c_0}\frac{1}{P_\sigma^{\alpha H}},
\end{aligned}
\tag{6}
$$

with the conditions $\sigma - 1 \geq 0$ and $\sigma - i \geq 0$ for $i \in [2,\sigma]$. Here, $P_\sigma^{\alpha H} = (\eta_{\sigma-1}^{\alpha H})^2\eta_{\rm BSM}^{\alpha}/\eta_\sigma^{\alpha H}$ is the success probability for entanglement swapping at nesting level σ, where $\eta_\sigma^{\alpha H} = \eta_{\sigma-1}^{\alpha H}/(2-\eta_{\sigma-1}^{\alpha H}\eta_{\rm BSM}^{\alpha})$ [37] and $\eta_{\rm BSM}^{\alpha} = (\eta_m)^2\eta_{\rm BSM}(\eta_d)^2$.

Using the same reasoning and calculation method, we can also derive a formula that relates the entanglement distribution time to the distribution distance for the heralded scheme with remote swapping, as follows:

$$
\begin{aligned}
T_\sigma^{\beta H} &= T_{0\sigma}^{\beta H} + T_{i\sigma}^{\beta H} + T_{L\sigma}^{\beta H} \\
&= 2^{(2^\sigma-\sigma)}\frac{L_0^\beta}{c_0}\frac{1}{P_0^{\beta H}}\prod_1^\sigma\frac{3-2(P_0^{\beta H})^{2^{\sigma-1}}}{2-(P_0^{\beta H})^{2^{\sigma-1}}} \\
&\quad + 2\times\sum_i^\sigma\left(\frac{2^i}{2}\frac{L_0^\beta}{c_0}\frac{1}{P_{i-1}^{\beta H}}\prod_i^\sigma\frac{3-2(P_{i-1}^{\beta H})^{2^{\sigma-i}}}{2-(P_{i-1}^{\beta H})^{2^{\sigma-i}}}\right) \\
&\quad + \frac{2^{\sigma+1}}{2}\frac{L_0^\beta}{c_0}\frac{1}{P_\sigma^{\beta H}}.
\end{aligned}
\tag{7}
$$

Here, $\sigma - 1 \geq 0$, $\sigma - i \geq 0$, and $i \in [2,\sigma]$. $P_0^{\beta H} = (p_{eD})^2(\eta_c)^2(\eta_{tR}^{\beta})^2\eta_{\rm BSM}(\eta_d)^2$ is the success probability of creating entanglement in one elementary link. The fiber transmittance for remote swapping is $\eta_{tR}^{\beta} = 10^{-(\alpha_{\rm fiber}\times 0.5L_0^{\beta})/10}$. The factor L_0^β/c_0 corresponds to the classical communication time over an elementary link of length L_0^β. $P_\sigma^{\beta H} = (\eta_{\sigma-1}^{\beta H})^2\eta_{\rm BSM}^{\beta}/\eta_\sigma^{\beta H}$ is the success probability for σ-level heralded entanglement swapping, with $\eta_\sigma^{\beta H} = \eta_{\sigma-1}^{\beta H}/(2-\eta_{\sigma-1}^{\beta H}\eta_{\rm BSM}^{\beta})$ [37]. Here, $\eta_{\rm BSM}^{\beta} = (\eta_m)^2(\eta_c)^2(\eta_{tR}^{\beta})^2\eta_{\rm BSM}(\eta_d)^2$ is the overall BSM efficiency at entanglement swapping for remote swapping. The terms $T_{0\sigma}^{\beta H}$, $T_{i\sigma}^{\beta H}$, and $T_{L\sigma}^{\beta H}$ represent, respectively, the waiting time until all elementary links of length L_0^β have successfully generated entanglement, the cumulative waiting time incurred during intermediate heralded swapping operations, and the waiting time for the last heralded swapping step to complete.

According to Eqs. (6)-(7), we can further obtain the entanglement distribution rate of the quantum repeater scheme when mode multiplexing is considered, [34] as follows:

$$
R_\sigma^{\alpha H} = \frac{M}{T_\sigma^{\alpha H}}, R_\sigma^{\beta H} = \frac{M}{T_\sigma^{\beta H}}. \tag{8}
$$

Here, M denotes the effective enhancement through multiplexing. In addition, to facilitate the explanation of the mechanism by which quantum repeaters overcome channel loss, we define a ratio function that compares entanglement distribution times for adjacent nesting levels σ. For the two quantum repeater schemes based on two-photon interference, these ratio functions are defined as follows:

$$
J_{\alpha H,\sigma,\sigma-1} = \frac{T_\sigma^{\alpha H}}{T_{\sigma-1}^{\alpha H}}, J_{\beta H,\sigma,\sigma-1} = \frac{T_\sigma^{\beta H}}{T_{\sigma-1}^{\beta H}}. \tag{9}
$$

4. Physical interpretation of quantum repeater

Using Eqs. (6)-(7), we obtain the theoretical curves of the two quantum repeater schemes at different nesting levels (e.g., $\sigma = 0, 1, \ldots, 4$) with realistic quantum device efficiencies, as illustrated in Figs. 2(a)-2(b). Furthermore, we plot the theoretical curves of the ratio functions for the two schemes using Eq. (9), as shown in Figs. 2(c)-2(d). These device efficiencies include the generation probability of EPS $p_{eD} = 0.046$, [43] the fiber attenuation coefficient $\alpha_{\rm fiber} = 0.146$ dB/km, [44] the QFC efficiency $\eta_c = 0.57$, [45] and the SPD efficiency $\eta_d = 0.95$. [46] In addition, the QM storage efficiency η_m is assumed to be time-dependent, i.e., $\eta_m = \eta_{m0}e^{-\tau/\tau_{\rm lifetime}}$, where $\eta_{m0} = 0.87$ and $\tau_{\rm lifetime} = 1$ ms. [47,48] For each scheme, the en-

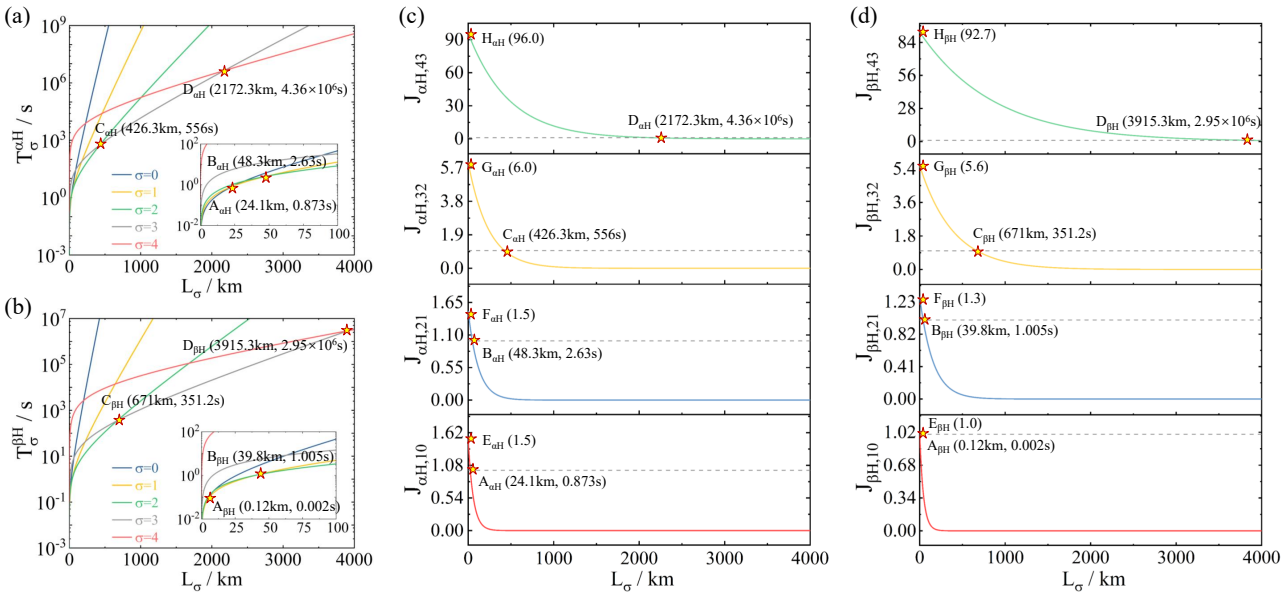


Fig. 2. Entanglement distribution time of two quantum repeater schemes. (a), (b) Theoretical curves of the heralded scheme with local swapping ($T_\sigma^{\alpha H}$) and the heralded scheme with remote swapping ($T_\sigma^{\beta H}$). Points $A_{\alpha H}$-$D_{\alpha H}$ and $A_{\beta H}$-$D_{\beta H}$ are crossover points of entanglement distribution times between adjacent σ values for these schemes, respectively. (c), (d) Ratio function graphs of the corresponding schemes. Points $A_{\alpha H}$-$D_{\alpha H}$ and $A_{\beta H}$-$D_{\beta H}$ represent crossover points when the ratio J equals 1. Points $E_{\alpha H}$-$H_{\alpha H}$ and $E_{\beta H}$-$H_{\beta H}$ denote values of the ratio J at $L_\sigma = 0.01$ km. The parameters are as follows: $p_{eD} = 0.046$, $\alpha_{\text{fiber}} = 0.146$ dB/km, $\eta_{\text{BSM}} = 1/2$, $\eta_c = 0.57$, $\eta_d = 0.95$, $\eta_{m0} = 0.87$, $\tau_{\text{lifetime}} = 1$ ms, and $c_{\text{fiber}} = 2 \times 10^5$ km/s.

tanglement distribution time as a function of distance exhibits crossover points between different nesting levels σ. These points, indicated in Figs. 2(a)-2(b), define characteristic distances L_σ at which increasing the nesting level (i.e., inserting additional repeater nodes) becomes advantageous for optimizing the performance of multi-node quantum repeaters.

Taking the heralded scheme with local swapping as an example, we illustrate this behavior. As shown in Fig. 2(a), direct entanglement distribution ($\sigma = 0$) is optimal for distances on the order of 24 km. For distances between $A_{\alpha H}$ (24.1 km) and $B_{\alpha H}$ (48.3 km), a single nesting level ($\sigma = 1$) minimizes the distribution time. Similarly, the intervals between $B_{\alpha H}$ and $C_{\alpha H}$, and between $C_{\alpha H}$ and $D_{\alpha H}$, correspond to optimal nesting levels of $\sigma = 2$ and $\sigma = 3$, respectively. This behavior reflects a fundamental trade-off between the characteristic distance and the number of nodes in quantum repeater design.

To illustrate this trade-off more specifically, we present the theoretical curve of the ratio function for the heralded scheme with local swapping, obtained using Eq. (9), as shown in Fig. 2(c). At very short distances (e.g., $L_\sigma = 0.01$ km), the ratio function values increase with the nesting level σ, as indicated by points $E_{\alpha H}$-$H_{\alpha H}$ in Fig. 2(c). This increase reflects the fact that adding more quantum nodes introduces additional initial system losses, which arise from the longer waiting time for elementary-link entanglement creation and from imperfect device efficiencies, including the EPS generation probability (p_{eD}), the QM storage efficiency (η_m), the QFC conversion efficiency (η_c), the SPD detection efficiency (η_d), and the BSM heralding probability (η_{BSM}). At these extremely short distances, the fiber transmittance η_{tR}^{α} is approximately unity. Thus, points $E_{\alpha H}$-$H_{\alpha H}$ represent the ratio of initial system losses between adjacent nesting levels σ.

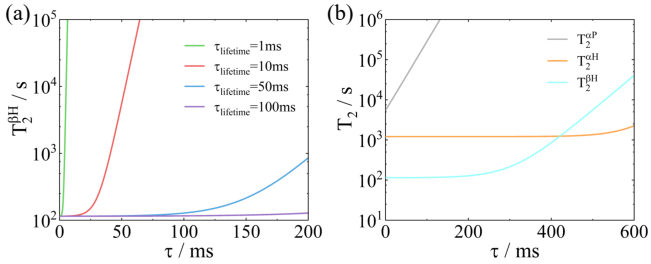


Fig. 3. Entanglement distribution time versus memory performance. (a) Distribution time versus storage time for the heralded scheme with remote swapping. The theoretical curves of distribution time as a function of storage time (τ) are shown for different values of τ_{lifetime}. (b) Comparison of distribution times for three repeater schemes. For $\tau_{\text{lifetime}} = 100$ ms, the distribution times of the heralded scheme with remote swapping ($T_2^{\beta H}$), the heralded scheme with local swapping ($T_2^{\alpha H}$), and the post-selected scheme with local swapping ($T_2^{\alpha P}$) are compared. The parameter values are $p_{eD} = 0.046$, $\alpha_{\text{fiber}} = 0.146$ dB/km, $\eta_{\text{BSM}} = 1/2$, $\eta_c = 0.57$, $\eta_d = 0.95$, $\eta_{m0} = 0.87$, $c_{\text{fiber}} = 2 \times 10^5$ km/s, $\sigma = 2$, and $L = 500$ km.

As the fiber distance increases, the channel loss becomes non-negligible. A higher nesting level σ divides the total distance L_σ into more segments, i.e., $L_\sigma/L_0^\alpha = 2^\sigma$ for local swapping, thereby reducing the fiber-channel loss, which is given by $\eta_{tR}^{\alpha} = 10^{-[\alpha_{\text{fiber}} \times 0.5(L_\sigma/2^\sigma)]}$. Thus, although a repeater archi-

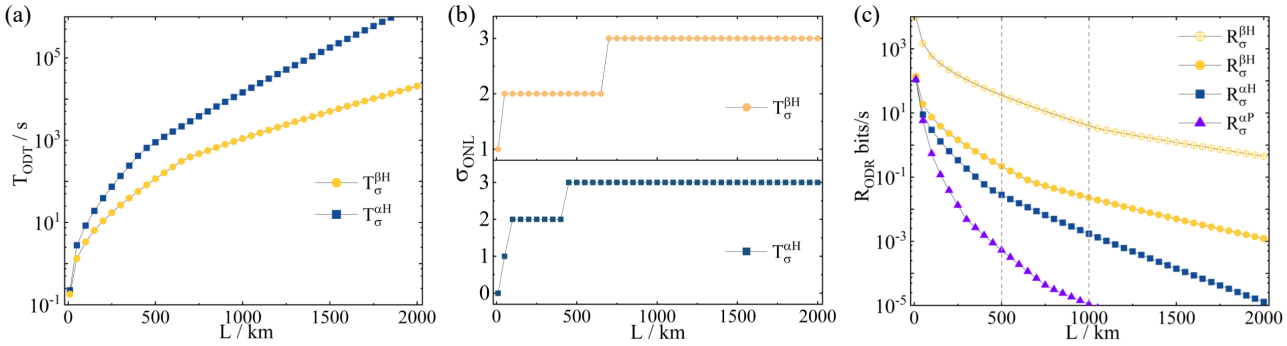


Fig. 4. Optimal nesting architectures and distribution rates of quantum repeater schemes. (a) Optimal distribution times under realistic device efficiencies. (b) Optimal nesting architectures under realistic device efficiencies. For the distribution distance L ranging from 10 km to 2000 km (e.g., 10 km, 50 km, 100 km, 150 km, …), the optimal distribution times (T_{ODT}) and optimal nesting architectures (σ_{ONL}) for two quantum repeater schemes are obtained through theoretical calculation. (c) Optimal distribution rate considering multiplexing ($M = 25$). The orange circles, blue squares, and purple triangles represent the optimal distribution rates of the heralded scheme with remote swapping ($R_\sigma^{\beta H}$), the heralded scheme with local swapping ($R_\sigma^{\alpha H}$), and the post-selected scheme with local swapping ($R_\sigma^{\alpha P}$), respectively, under realistic device efficiencies (i.e., $p_{eD} = 0.046$, $\alpha_{\mathrm{fiber}} = 0.146$ dB/km, $\eta_{\mathrm{BSM}} = 1/2$, $\eta_c = 0.57$, $\eta_d = 0.95$, $\eta_{m0} = 0.87$, $\tau_{\mathrm{lifetime}} = 1$ ms, and $c_{\mathrm{fiber}} = 2\times10^5$ km/s). However, the hollow yellow circles represent the optimal distribution rate of $R_\sigma^{\beta H}$ under near-ideal device efficiencies (i.e., $p_{eD} = 0.23$, $\alpha_{\mathrm{fiber}} = 0.091$ dB/km, $\eta_{\mathrm{BSM}} = 1/2$, $\eta_c = 0.95$, $\eta_d = 0.95$, $\eta_m = 0.95$, and $c_{\mathrm{fiber}} = 2\times10^5$ km/s). The gray dashed lines represent the comparison of the optimal distribution rates of these repeater schemes at distances of 500 km and 1000 km, respectively.

tecture with larger σ introduces more system loss at very short distances, it incurs less fiber-induced loss as L_σ increases. When the ratio function decays to unity, the corresponding distances mark the crossover points between entanglement distribution times for adjacent σ in Fig. 2(a). At these crossover points, the increase in distribution time caused by the initial system loss from adding more nodes is exactly balanced by the decrease caused by the reduction in fiber loss achieved through finer segmentation. Consequently, for distances L_σ beyond the characteristic distance corresponding to the intersection point, finer segmentation (i.e., larger σ) becomes the dominant factor in reducing the distribution time; conversely, for distances shorter than that, lower initial system loss (i.e., smaller σ) prevails. Furthermore, changes in parameter conditions shift these characteristic distances and the corresponding optimal nesting levels accordingly. Hence, these characteristic distances and optimal nesting levels provide quantitative guidelines for designing and scaling multi-node quantum repeater networks.

To investigate the influence of memory performance on the entanglement distribution time, we take the case of $L = 500$ km and $\sigma = 2$ as an example. By incorporating a time-dependent memory efficiency (e.g., $\eta_m = \eta_{m0}e^{-\tau/\tau_{\mathrm{lifetime}}}$) [48] into the analytical expression, we obtain the theoretical curves of the entanglement distribution time versus storage time for different memory lifetimes, as shown in Fig. 3(a). For longer memory lifetimes, the entanglement distribution time grows more slowly as the storage time increases. Therefore, continually improving the lifetime of quantum memories can help reduce the time required for successful entanglement distribution. In Fig. 3(b), we compare the distribution times of three repeater schemes when $\tau_{\mathrm{lifetime}} = 100$ ms. [49] Compared with the post-selected scheme ($T_2^{\alpha P}$), the heralded schemes ($T_2^{\alpha H}$ and $T_2^{\beta H}$) can reduce the time overhead when quantum memories with finite lifetimes are considered. For the two heralded schemes, the distribution-time curves for remote swapping and local swapping intersect as the storage time increases, corresponding to a characteristic storage time. When the storage time is shorter than this characteristic time, remote swapping achieves lower time overhead than local swapping. This advantage mainly arises because, under the same nested architecture and distribution distance, remote swapping enables finer segmentation than local swapping, thereby improving the fiber transmittance ($\eta_{tR}^{\beta} > \eta_{tR}^{\alpha}$). However, once the storage time exceeds this characteristic time, local swapping becomes more advantageous in reducing the distribution time. This reversal occurs mainly because remote swapping introduces additional losses during entanglement swapping, such as imperfect QFC efficiency and channel loss. As the storage time increases, the memory efficiency decays exponentially, making the overall BSM efficiency of remote swapping much lower than that of local swapping (i.e., $\eta_{\mathrm{BSM}}^{\beta} \ll \eta_{\mathrm{BSM}}^{\alpha}$). At the characteristic storage time, the reduction in distribution time achieved by finer segmentation to mitigate fiber loss is exactly offset by the increase in distribution time resulting from the lower overall BSM efficiency caused by the additional losses.

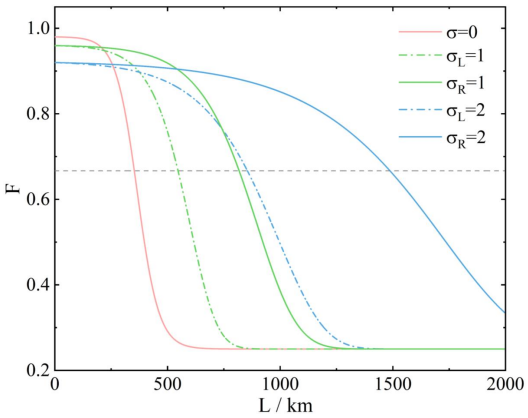


Fig. 5. Comparison of entanglement fidelity for quantum repeater schemes. The red solid line represents the entanglement fidelity of an elementary link. The green and blue solid lines represent the fidelities for remote swapping under two different entanglement swapping architectures ($\sigma_R = 1$ and $\sigma_R = 2$), whereas the green and blue dash-dotted lines represent those for local swapping under two different entanglement swapping architectures ($\sigma_L = 1$ and $\sigma_L = 2$). The gray dashed line indicates the fidelity threshold for successful teleportation. The parameters used are $p_{eD} = 0.23$, $\alpha_{\text{fiber}} = 0.091$ dB/km, $\eta_d = 0.95$, $\eta_c = 0.95$, $F_0 = 0.99$, $\eta_m = 0.95$, $\eta_{\text{BSM}} = 1/2$, and $d = 1 \times 10^{-5}$ (see Appendix D for the definitions of d and F_0).

5. Optimal nesting architecture of a quantum repeater channel

We compare the optimal entanglement distribution times of the two quantum repeater schemes under realistic device efficiencies, together with their corresponding optimal nesting architectures, as shown in Figs. 4(a) and 4(b). For the heralded schemes, remote swapping consistently outperforms local swapping in terms of distribution time, as illustrated by the comparison between $T_\sigma^{\alpha H}$ and $T_\sigma^{\beta H}$ in Fig. 4(a). This is mainly attributable to two factors. First, for identical nesting architectures, remote swapping enables finer segmentation than local swapping (e.g., $(2^{\sigma+1} - 1)/2^\sigma \in [1, 2)$). Second, for different nesting architectures, remote swapping introduces less initial system loss than local swapping. At $L = 500$ km, $T_\sigma^{\alpha H} \approx 889$ s, whereas $T_\sigma^{\beta H} \approx 115$ s, yielding a reduction factor of ∼7.7. This performance difference mainly originates from the initial system loss introduced by the repeater nodes. At $L = 500$ km, remote swapping requires only half the number of nodes ($\sigma_{\text{ONL}} = 2$, $n = 8$) compared with local swapping ($\sigma_{\text{ONL}} = 3$, $n = 16$) in Fig. 4(b). A larger number of quantum nodes n introduces greater initial system loss. Thus, although remote swapping ($L_\sigma/L_0^\beta = 7$) has slightly fewer segments than local swapping ($L_\sigma/L_0^\alpha = 8$), it incurs less initial system loss, which becomes the dominant factor. However, at $L = 1000$ km, $T_\sigma^{\alpha H} \approx 14542$ s, while $T_\sigma^{\beta H} \approx 1094$ s, corresponding to a reduction factor of ∼13.3. For the same nesting architecture ($\sigma_{\text{ONL}} = 3$, $n = 16$) in Fig. 4(b), remote swapping ($L_\sigma/L_0^\beta = 15$) divides the total distance into finer segments than local swapping ($L_\sigma/L_0^\alpha = 8$), thereby improving the fiber transmittance as given by $\eta_{tR}^{\beta/\alpha} = 10^{-[\alpha_{\text{fiber}} \times 0.5 L_0^{\beta/\alpha}]}$ and $\eta_{tR}^\beta > \eta_{tR}^\alpha$.

For short-distance entanglement distribution at $L = 100$ km with $M = 1$ under realistic device efficiencies, the distribution rates are $R_\sigma^{\beta H} \approx 0.3$ bits/s for the heralded scheme with remote swapping, $R_\sigma^{\alpha H} \approx 0.12$ bits/s for the heralded scheme with local swapping, and $R_\sigma^{\alpha P} \approx 0.02$ bits/s for the post-selected scheme with local swapping. However, these rates are relatively low, mainly because currently realized practical quantum devices have non-ideal efficiencies, including the extremely low EPS generation probability, the QM storage efficiency, the QFC efficiency, and so on. Therefore, to improve the distribution rate, we believe that efforts should focus mainly on two aspects: (i) improving realistic device efficiencies and (ii) employing mode-multiplexing techniques. [35,50] As shown in Fig. 4(c), using an effective multiplexing enhancement factor of $M = 25$, [51] we compare the optimal distribution rates of these schemes under realistic and near-ideal device efficiencies, respectively. The near-ideal device parameters used are $p_{eD} = 0.23$, [52] $\eta_m = 0.95$, [53] $\eta_c = 0.95$, [54] and $\alpha_{\text{fiber}} = 0.091$ dB/km. [55] The theoretical calculation for the post-selected scheme with local swapping is detailed in Appendix C. Under realistic device efficiencies, the heralded scheme with remote swapping consistently outperforms the other two schemes in terms of optimal distribution rate. At $L = 100$ km, $R_\sigma^{\alpha P} \approx 0.5$ bits/s and $R_\sigma^{\alpha H} \approx 3$ bits/s, whereas $R_\sigma^{\beta H} \approx 7.5$ bits/s, yielding an enhancement factor of ~ 15 relative to $R_\sigma^{\alpha P}$. At $L = 1000$ km, $R_\sigma^{\beta H}$ exceeds $R_\sigma^{\alpha H}$ and $R_\sigma^{\alpha P}$ by factors of ∼10 and ∼2000, respectively, with the three rates being ∼0.02 bits/s, ∼0.002 bits/s, and ∼0.00001 bits/s. When the near-ideal device efficiencies are considered, $R_\sigma^{\beta H} \approx 596$ bits/s at $L = 100$ km and $R_\sigma^{\beta H} \approx 4$ bits/s at $L = 1000$ km, yielding the enhancement factors of ~ 79.5 and ~ 200 relative to $R_\sigma^{\beta H}$ under realistic device efficiencies, respectively.

Although the above comparison focuses on the entanglement distribution rate, the entanglement fidelity of these schemes is also an important figure of merit. As shown in Fig. 5, we plot the theoretical curves of entanglement fidelity versus distance for remote swapping and local swapping under near-ideal device efficiencies; the derivation of the fidelity formula is given in Appendix D. As the nested architecture σ increases, the initial fidelity at short distances decreases, primarily because the larger number of nodes introduces additional loss into the link. At long distances, however, a larger nested architecture has an advantage over a smaller one in terms of

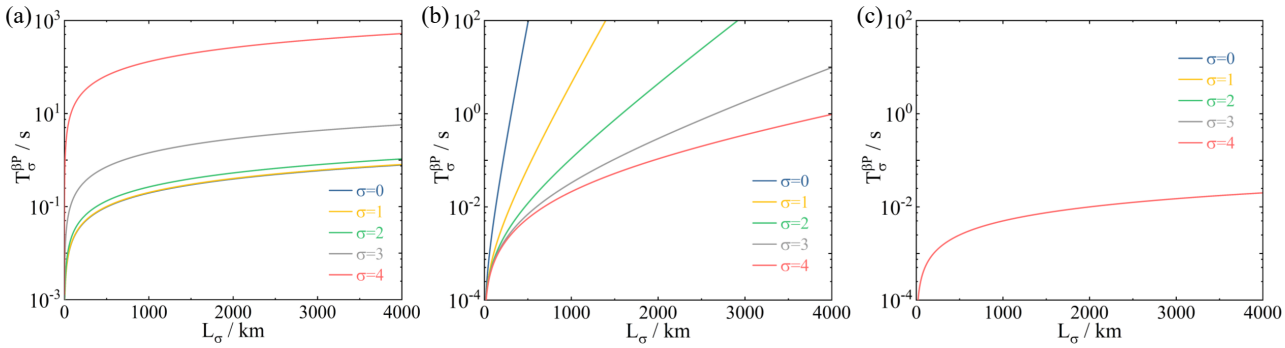


Fig. 6. Entanglement distribution time under extreme parameter conditions. (a)-(c) Distribution time for the heralded scheme with remote swapping under various ideal conditions, including zero channel loss, zero device loss, lossless Bell-state measurement, and a lossless repeater system. For each panel, the results are shown for nesting levels $\sigma = 0, 1, 2, 3, 4$. The parameters used are as follows: in (a), $p_{eD} = 0.23$, $\eta_{\text{BSM}} = 1/2$, $\eta_m = 0.95$, $\eta_c = 0.95$, $\alpha_{\text{fiber}} = 0$ dB/km, and $\eta_d = 0.95$; in (b), $p_{eD} = 1$, $\eta_{\text{BSM}} = 1$, $\eta_m = 1$, $\eta_c = 1$, $\alpha_{\text{fiber}} = 0.091$ dB/km, and $\eta_d = 1$; and in (c), $p_{eD} = 1$, $\eta_{\text{BSM}} = 1$, $\eta_m = 1$, $\eta_c = 1$, $\alpha_{\text{fiber}} = 0$ dB/km, and $\eta_d = 1$.

fidelity. When the fidelity threshold for successful teleportation is taken into account (e.g., $F_{threshold} = \frac{2}{3}$) [56], there is a trade-off in quantum repeater design between the initial fidelity, which is affected by the nested architecture, and the distribution distance. In addition, for the same nested architecture, remote swapping can mitigate the decline in fidelity with distance compared with local swapping, thereby facilitating entanglement distribution over longer distances. This is mainly because, for the same nested architecture and distance, remote swapping enables finer segmentation than local swapping, thereby reducing channel loss. These results allow us to determine the optimal entanglement fidelity under near-ideal device efficiencies. In practice, however, for quantum repeater schemes based on two-photon interference, an EPS with both a high entangled-photon-pair generation probability and negligible noise is desirable. Unfortunately, currently available spontaneous parametric down-conversion (SPDC) sources that generate polarization-entangled photon pairs introduce multi-photon-pair noise at high generation probabilities, thereby degrading the fidelity of the entangled photon pairs. [57] Thus, to resolve the trade-off between the generation probability and multi-photon noise, a near-ideal photon-number-resolving detector scheme [58] or a multiplexing architecture at low generation probability [59] is provided. For SPDC sources, Appendix E discusses the trade-off between generation probability and fidelity, as well as its implications for entanglement-distribution fidelity.

6. Analysis of quantum repeater under extreme parameter conditions

Under extreme parameter conditions, we plot the theoretical curves of the entanglement distribution time as a function of distance for the heralded scheme with remote swapping at nesting levels $\sigma = 0, 1, 2, 3, 4$, as illustrated in Figs. 6(a)-6(c). When channel loss is set to zero while other losses are retained, the curves for different nesting levels exhibit no crossover points, and a higher nesting level yields a longer distribution time, as depicted in Fig. 6(a). This behavior arises because a larger nesting level requires more quantum nodes, which introduces additional initial system losses due to imperfect device efficiencies and finite BSM heralding efficiency. In the absence of channel loss, these initial system losses become the dominant factor governing the distribution time over the entire range of distances.

When the channel loss is nonzero while all other losses vanish, a higher nesting level yields a shorter entanglement distribution time over the entire distance range, as shown in Fig. 6(b). This occurs because, in the absence of initial system loss, a larger nesting architecture divides the distance into finer segments, thereby reducing the impact of channel loss on the distribution time. This case clearly illustrates the limiting performance of quantum repeaters when they are affected solely by channel loss. Naturally, when all losses are set to zero (e.g., a lossless repeater system), the theoretical curves of the distribution time versus distance for different nesting architectures become identical, as depicted in Fig. 6(c); in this case, the distribution time is governed only by the classical communication time. Thus, under these extreme parameter conditions, the behavior predicted by our derived Eq. (7) for the heralded scheme with remote swapping is consistent with theoretical expectations.

7. Conclusion and outlook

In this work, we have calculated the entanglement distribution time for quantum repeater schemes that combine local or remote swapping with a heralded scheme. A key result of our work is an analytical formula that explicitly relates the distribution time to the transmission distance, providing a general tool for assessing the performance of such repeater architectures. Guided by this formula, we have elucidated the physical mechanism by which quantum repeaters mitigate the detrimental effects of channel loss in long-distance fiber transmission. Considering a realistic quantum memory, we have presented theoretical curves showing the effect of finite memory lifetime on the entanglement distribution time. Through a systematic comparison of the optimal distribution times across distances up to thousands of kilometers, we have determined the optimal nesting configurations for a single-repeater channel. Considering mode multiplexing, we have compared the optimal distribution rates of the heralded schemes and the post-selected scheme at various distances under realistic device efficiencies. Furthermore, by comparing the entanglement fidelity of these schemes, we find that remote swapping can mitigate the decline in fidelity with distance more effectively than local swapping under the same nested architecture. Finally, by examining the limiting cases of zero channel loss, zero device loss, and completely lossless repeater systems, we have found the fundamental performance bounds for quantum repeaters. Our work expands the theoretical framework for quantum repeater protocols and deepens the understanding of their operational dynamics, thereby supporting the future development of scalable quantum networks.

This work establishes quantitative guidelines for the design of large-scale quantum repeater networks, including optimal node placement and architecture selection at continental distances. Several directions may further improve repeater-based quantum communication. First, beyond the binary-tree segmentation considered here, alternative network topologies could be explored, [60–62] particularly in regimes where entanglement generation and swapping are performed concurrently, potentially reducing both node requirement and distribution time. Second, hybrid quantum network architectures that integrate fiber-based repeaters with free-space or satellite links may overcome the limitations of fiber loss and enable global-scale connectivity. [63,64] Third, continued advances in key hardware components, including entangled photon sources, [65–67] quantum memories, [68–70] quantum transducers, [71–73] and low-loss optical fibers, [74] will be essential for approaching the ultimate performance limits of quantum repeater networks.

Appendix A: Quantum repeater schemes with two-photon interference

For a quantum repeater scheme based on single-photon interference, all Bell state measurements (BSMs) in Fig. 7 employ the scheme shown in illustration (ii). When either single-photon detector D1 or D2 in a BSM clicks, entanglement is successfully established in the corresponding elementary link, yielding photon-number entangled states of the form $|1_n, 0_{n+1}\rangle$ or $|0_n, 1_{n+1}\rangle$, where the subscript n labels the quantum nodes. Achieving such photon-number entanglement requires that, in each elementary link, only one of the entangled photon sources is excited to generate entangled photon pairs, thereby limiting the excitation probability of the entangled photon sources to approximately one percent. After all swapping operations are completed, long-distance entanglement is established in the form of photon-number entangled states between the beginning and ending nodes, i.e., $|1_B, 0_E\rangle$ and $|0_B, 1_E\rangle$, with subscripts B and E denoting the beginning and ending nodes, respectively.

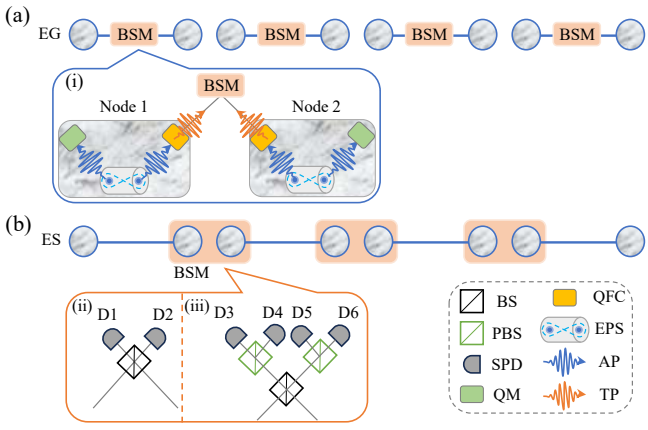


Fig. 7. Quantum repeater schemes with single-photon interference and two-photon interference. (a) Entanglement generation (EG) of every elementary link. In illustration (i), every elementary link consists of one BSM station and two nodes. Every node includes the EPS, QFC, and QM. (b) Entanglement swapping (ES) is completed when entangled states in all elementary links have been created. Here, if all BSMs are implemented via the single-photon interference scheme (illustration (ii)), photon-number entanglement can be achieved. Conversely, if all BSMs rely on the two-photon interference scheme (illustration (iii)), polarization entanglement can be realized. BSM: Bell-state measurement. PBS: Polarization beam splitter. BS: Beam splitter. SPD: Single-photon detector. QM: Quantum memory. QFC: Quantum frequency converter. EPS: Entangled photon source. AP: Photon in the atomic operating band. TP: Telecom-wavelength photon.

For a quantum repeater scheme based on two-photon interference, all BSMs in Fig. 7 employ the configuration shown in illustration (iii). As shown in illustration (i)

of Fig. 7, when the entangled photon sources at nodes 1 and 2 simultaneously generate polarization-entangled photon pairs, i.e., $|\Phi_1\rangle = 1/\sqrt{2}(|H\rangle_{1L}|V\rangle_{1R} + |V\rangle_{1L}|H\rangle_{1R})$ and $|\Phi_2\rangle = 1/\sqrt{2}(|H\rangle_{2L}|V\rangle_{2R} + |V\rangle_{2L}|H\rangle_{2R})$, the blue photons at nodes 1 and 2 are stored in quantum memories (QM_1 and QM_2), respectively. The subscripts 1L and 1R (2L and 2R) denote the left and right blue photons at node 1 (node 2), respectively. Meanwhile, their partners are converted to telecom-wavelength photons (orange) via quantum frequency converters (QFCs) and transmitted through fiber channels to a BSM station. So, the overall entangled state of the two nodes is $|\Phi_{12}\rangle = 1/2(|H\rangle_{1L}|V\rangle_{1R}|H\rangle_{2L}|V\rangle_{2R} + |H\rangle_{1L}|V\rangle_{1R}|V\rangle_{2L}|H\rangle_{2R} + |V\rangle_{1L}|H\rangle_{1R}|H\rangle_{2L}|V\rangle_{2R} + |V\rangle_{1L}|H\rangle_{1R}|V\rangle_{2L}|H\rangle_{2R})$.

If the orange photons from the two nodes have identical polarizations—either $|V\rangle_{1R}|V\rangle_{2L}$ or $|H\rangle_{1R}|H\rangle_{2L}$—then only a single detector at the BSM station (one of D3-D6) registers a click, indicating the detection of two photons. In this case, however, the states $|V\rangle_{1R}|V\rangle_{2L}$ and $|H\rangle_{1R}|H\rangle_{2L}$ can be distinguished by which detector fires: D4 or D5 for the former, and D3 or D6 for the latter. Consequently, no entangled state is generated. Conversely, when the orange photons are orthogonally polarized—$|V\rangle_{1R}|H\rangle_{2L}$ or $|H\rangle_{1R}|V\rangle_{2L}$—exactly two of the four BSM detectors click simultaneously (e.g., D3 and D4, D5 and D6, D3 and D5, or D4 and D6). Such an event projects the blue photons onto the orthogonal polarization state, i.e., $|H\rangle_{1L}|V\rangle_{2R}$ or $|V\rangle_{1L}|H\rangle_{2R}$. Therefore, the orthogonal-polarization case in the heralded scheme enables long-distance entanglement distribution for quantum repeaters based on two-photon interference. When every BSM station in all elementary links registers a double-detector click, entanglement is independently established in every elementary link. Thus, each elementary link produces entangled states of either $|H\rangle_n|V\rangle_{n+1}$ or $|V\rangle_n|H\rangle_{n+1}$. Since these two states correspond to the Fock states $|1_n, 0_{n+1}\rangle$ and $|0_n, 1_{n+1}\rangle$, respectively, the theoretical framework for quantum repeater protocols based on single-photon interference becomes directly applicable to the long-distance distribution of photon-photon entanglement along a single chain. Upon completion of nested entanglement swapping, long-distance entanglement is established as a polarization-entangled state between the beginning and ending nodes, i.e., $1/\sqrt{2}(|H\rangle_B|V\rangle_E + |V\rangle_B|H\rangle_E)$.

Appendix B: Waiting time for success in two independent events

When the entanglement creation of an elementary link is treated as an independent event, the waiting time for an elementary link with success probability P_0 follows a geometric distribution (in units of L_0/c), [42] i.e.,

$$p(t) = (1 - P_0)^{t-1} P_0. \tag{B1}$$

Here, L_0/c is the classical communication time for an elementary link. Thus, for an elementary link with successful entanglement creation, its average waiting time can be written as

$$\langle t \rangle = \sum_{t=0}^{\infty} t p(t) = \sum_{t=0}^{\infty} t(1 - P_0)^{t-1} P_0 = \frac{1}{P_0}. \tag{B2}$$

To attempt the first entanglement swapping, the entanglement creations of two adjacent elementary links must both succeed. We treat these two elementary links, which require successful entanglement creation, as two independent events. Hence, the corresponding waiting time is the maximum of the waiting times of the two independent events, each following the distribution given by an elementary link. Now, we define the distribution of the waiting time for both independent events to succeed as $\tilde{p}(t)$, and the corresponding average waiting time as $\langle \tilde{t} \rangle$. So, taking into account all cases in which we have to wait until time t for at least one of the two links to succeed, the distribution is

$$\tilde{p}(t) = p(t)^2 + 2p(t) \sum_{k=1}^{t-1} p(k). \tag{B3}$$

The corresponding average waiting time is

$$\begin{aligned} \langle \tilde{t} \rangle =& \sum_{t=0}^{\infty} t \tilde{p}(t) \\ =& 2 \sum_{t=0}^{\infty} t p(t) \Big(\sum_{k=1}^{t-1} p(k) + \frac{1}{2} p(t) \Big). \end{aligned} \tag{B4}$$

When substituting Eq. (B1) into Eq. (B3) and simplifying, we obtain the explicit expression for $\tilde{p}(t)$ in terms of P_0, as follows:

$$\begin{aligned} \tilde{p}(t) =& P_0^2 (1 - P_0)^{2t-2} + 2P_0 (1 - P_0)^{t-1} \\ & \times [1 - (1 - P_0)^{t-1}]. \end{aligned} \tag{B5}$$

By substituting Eq. (B5) into Eq. (B4), the average waiting time for both independent events to succeed is further simpli-

fied to

$$\begin{aligned}\langle\tilde{t}\rangle &= \sum_{t=0}^{\infty} t\tilde{p}(t) \\ &= \sum_{t=0}^{\infty} tP_0^2(1-P_0)^{2t-2} + \sum_{t=0}^{\infty} 2tP_0(1-P_0)^{t-1} \\ &- \sum_{t=0}^{\infty} 2tP_0(1-P_0)^{2t-2}.\end{aligned} \tag{B6}$$

Considering Eq. (B2), we can obtain $\sum_{t=0}^{\infty} t(1-P_0)^{t-1} = 1/P_0^2$ and $\sum_{t=0}^{\infty} t(1-P_0)^{2t-2} = 1/(2P_0 - P_0^2)^2$. Thus, Eq. (B6) is finally simplified to

$$\begin{aligned}\langle\tilde{t}\rangle =& \frac{2}{P_0} + (P_0^2 - 2P_0)\sum_{t=0}^{\infty} t(1-P_0)^{2t-2} \\ =& \frac{3-2P_0}{(2-P_0)P_0}.\end{aligned} \tag{B7}$$

In addition, Eq. (B7) is also referred to as the average number of tries for both independent events to succeed, [37] i.e., $\nu_0 = \frac{3-2P_0}{(2-P_0)P_0}$. So, according to Eq. (B2) and Eq. (B7), we can respectively obtain that the average waiting time for a single elementary link to successfully create entanglement is $\langle t\rangle = \frac{1}{P_0}$, and the average waiting time for two independent elementary links to successfully create entanglement is $\langle\tilde{t}\rangle = \frac{3-2P_0}{(2-P_0)P_0} = \langle t\rangle\nu_0 P_0$.

According to Eq. (B4), we can obtain that the expression inside the parentheses (e.g., $\sum_{k=1}^{t-1} p(k) + \frac{1}{2}p(t)$) is bounded by 1. Thus, one must have

$$\langle\tilde{t}\rangle \leq 2\langle t\rangle. \tag{B8}$$

One also has

$$\langle t\rangle \leq \langle\tilde{t}\rangle. \tag{B9}$$

Since waiting for two independent successes has to take at least as long as waiting for a single success, we define

$$f \equiv \frac{\langle\tilde{t}\rangle}{\langle t\rangle} = \frac{3-2P_0}{2-P_0} \tag{B10}$$

with $1 \leq f \leq 2$. Here, f is understood as the coefficient given by the ratio of the average waiting time for two independent events both to succeed to that for one event alone.

Now, using Eq. (B7), we consider the average waiting time for the successful entanglement creation of j elementary links ($j = 2^\sigma$, $\sigma = 1, 2, 3, \ldots$), as follows:

$$\langle\tilde{t}_{0\sigma}\rangle = \frac{1}{P_0}\prod_{1}^{\sigma}\frac{3-2(P_0)^{2^{\sigma-1}}}{2-(P_0)^{2^{\sigma-1}}}. \tag{B11}$$

For example, 2^3 elementary links are considered. According to Eq. (B11), the average waiting time is

$$\langle\tilde{t}_{03}\rangle = \frac{1}{P_0}\frac{3-2P_0}{2-P_0}\frac{3-2(P_0)^2}{2-(P_0)^2}\frac{3-2(P_0)^4}{2-(P_0)^4}. \tag{B12}$$

We explain the meaning of Eq. (B12) as follows. The average waiting time for two independent elementary links both to succeed is $\frac{1}{P_0}\frac{3-2P_0}{2-P_0}$. On this basis, we further consider two additional elementary links both succeeding, whose average waiting time is $\frac{1}{P_0}\frac{3-2P_0}{2-P_0}\frac{3-2(P_0)^2}{2-(P_0)^2}$. Here, two combinations, each consisting of two elementary links, are treated as two independent events. Finally, building upon the previous results, we further consider four additional elementary links all succeeding, whose average waiting time is $\frac{1}{P_0}\frac{3-2P_0}{2-P_0}\frac{3-2(P_0)^2}{2-(P_0)^2}\frac{3-2(P_0)^4}{2-(P_0)^4}$. Here, two combinations, each consisting of four elementary links, are treated as two independent events. Hence, based on the successful entanglement creation of all elementary links, we also consider the accumulated average waiting time for entanglement swapping operations at different nesting levels in the same manner as described above.

Appendix C: Theoretical calculation for the post-selected scheme with local swapping

For the post-selected scheme with local swapping, the total distance L is equally divided into 2^σ segments of length $L_0^\alpha = L/2^\sigma$, where σ denotes the nesting level of entanglement swapping. Let us now consider the case of heralding an entangled state with orthogonal polarization. When entanglement is successfully created in an elementary link, e.g., between nodes 1 and 2, the time required for successful entanglement distribution in that link is [42]

$$T_0 = \frac{L_0^\alpha}{c_0}\frac{1}{P_0}, \tag{C1}$$

where P_0 is the success probability for creating entanglement in an elementary link. Specifically, $P_0 = 2p_{eS}\eta_c\eta_{tR}^\alpha\eta_d$ for the BSM based on single-photon interference, and $P_0 = (p_{eD})^2(\eta_c)^2(\eta_{tR}^\alpha)^2\eta_{\rm BSM}(\eta_d)^2$ for the BSM based on two-photon interference considered in this work. Here, p_{eD} (p_{eS}) denotes the generation probability of entangled photon pairs (the probability of single atomic excitation). The fiber transmittance

for local swapping is given by $\eta_{tR}^{\alpha} = 10^{-(\alpha_{\text{fiber}}\times 0.5 L_0^{\alpha})/10}$. Furthermore, η_c, η_m, and η_{BSM} represent the conversion efficiency of QFC, the storage efficiency of QM, and the heralding efficiency of BSM, respectively. The factor L_0^{α}/c_0 corresponds to the classical communication time over one elementary link of length L_0^{α}.

Now, we consider the first post-selected entanglement swapping between elementary links 1 (nodes 1 and 2) and 2 (nodes 3 and 4) for the case $\sigma = 1$. When two independent binomial events (i.e., entanglement creation or swapping), each with success probability P_σ, are both required to succeed, the average number of tries is given by $\nu_\sigma = \frac{3-2P_\sigma}{(2-P_\sigma)P_\sigma}$. [37,42] Hence, for entanglement creation in elementary links 1 and 2, each with probability P_0, the average number of tries is $\nu_0 = \frac{3-2P_0}{(2-P_0)P_0}$. From Eq. (C1), the average waiting time for both elementary links to succeed is $T_0\nu_0 P_0$, as shown in Appendix B. Consequently, when the entanglement swapping operation is treated as instantaneous (i.e., the swapping time overhead is neglected), the time required to establish entanglement is [42]

$$T_1 = \frac{L_0^{\alpha}}{c_0}\nu_0\frac{1}{P_1}, \tag{C2}$$

where $P_1 = (1/2)(\eta/\eta_1)$ is the success probability of the first post-selected entanglement swapping, with $\eta_1 = 1/(2-\eta)$. Here, η is given by $\eta_m\eta_d$ for the BSM based on single-photon interference, and by $(\eta_m)^2\eta_{\text{BSM}}(\eta_d)^2$ for the BSM based on two-photon interference considered in this work. Generalizing to σ-level post-selected entanglement swapping, the total time required to successfully distribute entanglement between the beginning and ending nodes is [42]

$$T_\sigma = \frac{L_0^{\alpha}}{c_0}\nu_0\nu_1\nu_2\ldots\nu_{\sigma-1}\frac{1}{P_\sigma}. \tag{C3}$$

Here, $P_\sigma = (1/2)[(\eta_{\sigma-1})^2\eta/\eta_\sigma]$ is the success probability of σ-level entanglement swapping, with $\eta_\sigma = \eta_{\sigma-1}/(2-\eta_{\sigma-1}\eta)$. The factor 1/2 arises from the probability that the entangled states generated in neighboring links are compatible with the subsequent entanglement swapping. The factor η_σ represents the overall efficiency, incorporating the efficiencies of the relevant quantum devices and the probability of heralding Bell states. Eq. (C3) inherits this instantaneous-swapping approximation.

For the BSM with single-photon interference, each elementary link produces entangled states of two types: $|1_n, 0_{n+1}\rangle$ and $|0_n, 1_{n+1}\rangle$, where the subscript n labels the quantum nodes. When $\sigma = 1$, adjacent elementary links can exhibit four possible combinations of these entangled states: $(|1_1, 0_2\rangle, |1_3, 0_4\rangle)$, $(|1_1, 0_2\rangle, |0_3, 1_4\rangle)$, $(|0_1, 1_2\rangle, |0_3, 1_4\rangle)$, and $(|0_1, 1_2\rangle, |1_3, 0_4\rangle)$. Among these, only two, i.e., $(|1_1, 0_2\rangle, |1_3, 0_4\rangle)$ and $(|0_1, 1_2\rangle, |0_3, 1_4\rangle)$, are compatible with the first post-selected entanglement swapping ($\sigma = 1$). An analogous situation holds for higher nesting levels σ. Consequently, the success probability of entanglement swapping (P_σ) contains a factor of 1/2. When the BSM based on single-photon interference is employed in the quantum repeater protocol, the elementary-link entanglement-creation probability and the entanglement-swapping success probability are given respectively by $P_{0S}^{\alpha P} = 2p_{eS}\eta_c\eta_{tR}^{\alpha}\eta_d$ and $P_{\sigma S}^{\alpha P} = (1/2)((\eta_{\sigma-1,S}^{\alpha P})^2\eta_S^{\alpha P}/\eta_{\sigma S}^{\alpha P})$, where $\eta_{\sigma S}^{\alpha P} = \eta_{\sigma-1,S}^{\alpha P}/(2-\eta_{\sigma-1,S}^{\alpha P}\eta_S^{\alpha P})$, $\eta_S^{\alpha P} = \eta_m\eta_d$, and $\eta_{0S}^{\alpha P} = 1$. Because the quantum repeater scheme based on single-photon interference requires suppression of multi-photon events, the excitation probability p_{eS} is limited to approximately 0.01. Under these conditions, Eq. (C3) can be further approximated as $T_{\sigma S}^{\alpha P} \approx (L_0^{\alpha}/c_0)(3/2)^{\sigma}/(P_{0S}^{\alpha P}P_{1S}^{\alpha P}\ldots P_{\sigma S}^{\alpha P})$. [37]

For the BSM based on two-photon interference, the success probability of entanglement creation in an elementary link is $P_0^{\alpha P} = (p_{eD})^2(\eta_c)^2(\eta_{tR}^{\alpha})^2\eta_{\text{BSM}}(\eta_d)^2$, and the success probability for entanglement swapping at nesting level σ is $P_\sigma^{\alpha P} = (1/2)[(\eta_{\sigma-1}^{\alpha P})^2\eta_{\text{BSM}}^{\alpha}/\eta_\sigma^{\alpha P}]$, with $\eta_\sigma^{\alpha P} = \eta_{\sigma-1}^{\alpha P}/(2-\eta_{\sigma-1}^{\alpha P}\eta_{\text{BSM}}^{\alpha})$ and $\eta_{\text{BSM}}^{\alpha} = (\eta_m)^2\eta_{\text{BSM}}(\eta_d)^2$. In this scheme, the entangled states $|H\rangle_n|V\rangle_{n+1}$ and $|V\rangle_n|H\rangle_{n+1}$ are analogous to the photon-number entangled states $|1\rangle_n|0\rangle_{n+1}$ and $|0\rangle_n|1\rangle_{n+1}$, respectively. By replacing P_0 and P_σ in Eq. (C3) with $P_0^{\alpha P}$ and $P_\sigma^{\alpha P}$, we obtain the entanglement distribution time for the quantum repeater protocol based on two-photon interference: $T_\sigma^{\alpha P} = \frac{L_0^{\alpha}}{c_0}\nu_0^{\alpha P}\nu_1^{\alpha P}\nu_2^{\alpha P}\ldots\nu_{\sigma-1}^{\alpha P}\frac{1}{P_\sigma^{\alpha P}}$. Here, $\nu_i^{\alpha P} = \frac{3-2P_i^{\alpha P}}{(2-P_i^{\alpha P})P_i^{\alpha P}}$ is the average number of tries required for two independent binomial events (e.g., entanglement creation or swapping), each with probability $P_i^{\alpha P}$, to both succeed, with $i \in [0, \sigma-1]$. When mode multiplexing is considered, the entanglement distribution rate is given by $R_\sigma^{\alpha P} = M/T_\sigma^{\alpha P}$.

Appendix D: Entanglement fidelity of quantum repeater schemes

For quantum repeater schemes based on two-photon interference, each EPS generates a polarization-entangled state $|\Phi^+\rangle = 1/\sqrt{2}(|H\rangle|V\rangle + |V\rangle|H\rangle)$, which is one of the four Bell states. For a realistic EPS (such as an SPDC source), the fidelity of the generated entangled state is assumed to be F_0. When F_0 is not perfect, a symmetrized state (e.g., a Werner

state) is given by [75]

$$W_F = F_0|\Phi^+\rangle\langle\Phi^+| + \frac{1-F_0}{3}|\Phi^-\rangle\langle\Phi^-| + \frac{1-F_0}{3}|\Psi^+\rangle\langle\Psi^+| + \frac{1-F_0}{3}|\Psi^-\rangle\langle\Psi^-|, \tag{D1}$$

where $|\Phi^-\rangle = 1/\sqrt{2}(|H\rangle|V\rangle - |V\rangle|H\rangle)$ and $|\Psi^\pm\rangle = 1/\sqrt{2}(|H\rangle|H\rangle \pm |V\rangle|V\rangle)$. The first term represents the desired entanglement generated by the EPS, whereas the latter three terms correspond to the erroneous states caused by imperfect fidelity.

We now show that the quantum repeater scheme takes two Werner pairs of fidelity F_0 as input, performs a swapping operation on the particles at a BSM (e.g., $\sigma = 0$), and yields a new pair with fidelity [26,76,77]

$$F = \frac{1}{4}(1 + 3p_1p_2\frac{4\eta^2-1}{3}\frac{4F_0-1}{3}\frac{4F_0-1}{3}). \tag{D2}$$

Here, the parameter η represents the quality of the projection onto the basis states and is assumed to be perfect (i.e., $\eta = 1$). Since a BSM based on two-photon interference is considered, we assume perfect single-qubit operations (i.e., $p_1 = 1$) and focus solely on the imperfection of two-qubit operations (p_2). Thus, due to the imperfect operation, the average fidelity of the two-qubit operation is given by [78–80]

$$\bar{F} = p_2 + \frac{1-p_2}{D}, \tag{D3}$$

where $D = 2^a$ is the dimension of the relevant subspace of the Hilbert space for a qubits.

For a two-qubit system, the relationship between the average fidelity and the parameter p_2 is expressed as $\bar{F} = \frac{1}{4} + \frac{3}{4}p_2$. Furthermore, the average fidelity can be interpreted as the correctness rate of performing a BSM within a quantum repeater link. Hence, a simplified model relates the average fidelity to the link where the BSM is performed, namely, $\bar{F} \approx \frac{\eta_L+0.25d}{\eta_L+d}$. Here, η_L and d denote the total transmittance and the total dark count probability of the communication link, respectively. The total dark count probability is $d = R_d t_w$, where R_d is the dark-count rate and t_w is the detection-window duration [81]. For short distances (e.g., $\eta_L \gg d$), we obtain $\bar{F} \approx 1$; however, when $\eta_L \ll d$, $\bar{F} \approx 0.25$, which represents the lower bound of fidelity induced by fully random noise in a two-qubit entangled system. Thus, the parameter p_2 can be written as

$$p_2 = \frac{4}{3}(\frac{\eta_L+0.25d}{\eta_L+d} - \frac{1}{4}). \tag{D4}$$

By substituting Eq. (D4) into Eq. (D2) and simplifying, the fidelity for long-distance entanglement distribution is given by

$$F = \frac{1}{4}(1 + 4(\frac{\eta_L+0.25d}{\eta_L+d} - \frac{1}{4})\frac{4F_0-1}{3}\frac{4F_0-1}{3}). \tag{D5}$$

Thus, the fidelity of the entangled state generated by the $\sigma = 0$ link depends primarily on the fidelity of the entangled photon pairs (F_0), the total transmittance (η_L), and the total dark count probability (d) of the communication link. For $\sigma = 0$, $\eta_L = p_{eD}^2\eta_c^2\eta_{tR}^2\eta_{\mathrm{BSM}}\eta_d^2$, where η_{tR} is the fiber transmittance. To determine the fidelity of the entangled state generated at higher nesting levels, one can simply recursively iterate Eq. (D5), with η_L replaced by the success probability at the entanglement-swapping operation.

Appendix E: Impact of SPDC sources on entanglement fidelity

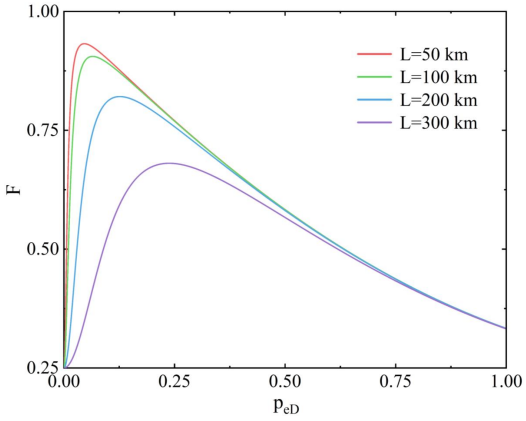


Fig. 8. Entanglement fidelity (F) versus generation probability (p_{eD}) for the SPDC source. For entanglement generation in a single elementary link ($\sigma = 0$), theoretical curves of F versus p_{eD} are presented for various distances. The parameters used are $\alpha_{\mathrm{fiber}} = 0.091$ dB/km, $\eta_d = 0.95$, $\eta_c = 0.95$, $\eta_m = 0.95$, $\eta_{\mathrm{BSM}} = 1/2$, and $d = 1 \times 10^{-5}$.

Under ideal conditions in which multimode effects are neglected, the quantum state generated by the SPDC process is a two-mode squeezed vacuum state, whose Fock-state expansion is [82]

$$|\Psi_{\mathrm{SPDC}}\rangle = \sqrt{1-|\lambda|^2}\sum_{n=0}^{\infty}\lambda^n|n,n\rangle. \tag{E1}$$

Here, $|\lambda|^2$ is the squared magnitude of the squeezing parameter and is proportional to the pump intensity. When pulsed pump light is launched into an SPDC crystal, the probability of generating entangled photon pairs is proportional to $|\lambda|^2$; that is, $p_{eD} = |\lambda|^2$. [83] Thus, the probability that the SPDC

source generates n entangled photon pairs is

$$P(n) = (1 - p_{eD})p_{eD}^{n}. \tag{E2}$$

According to Eq. (E2), when the SPDC crystal is excited by pulsed pump light, the total probability of generating entangled photon pairs, the probability of generating exactly one entangled photon pair, and the probability of generating multiple entangled photon pairs are respectively given by

$$P_{total} = \sum_{n=1}^{\infty} P(n) = p_{eD}, P_1 = (1 - p_{eD})p_{eD}, P_{n\geq 2} = p_{eD}^2. \tag{E3}$$

When the SPDC source produces exactly one photon pair, the system is in an ideal polarization-entangled state. Under perfect measurement conditions, its fidelity is $F_1 = 1$. However, when the SPDC source produces two or more photon pairs, because conventional threshold detectors cannot resolve the photon number, these multi-pair events are misidentified as single-pair events and are included in the coincidence counts. The equivalent fidelity of the multi-pair photon state relative to the ideal single-pair state is $F_{n\geq 2} = 0.5$. When only multi-pair photon noise is taken into account, the fidelity of the entangled photon pairs generated by the SPDC source can be expressed as

$$F_0 = \frac{P_1 \times F_1 + P_{n\geq 2} \times F_{n\geq 2}}{P_{total}} = 1 - 0.5p_{eD}. \tag{E4}$$

According to the above equation, the generation probability of entangled photon pairs exhibits a linear negative correlation with their fidelity. In the weak pump region ($p_{eD} \ll 1$), multi-pair photon events are extremely rare, and the fidelity is very close to 1; however, in the strong pump region, multi-pair photon events dominate, and the fidelity approaches 0.5.

By substituting Eq. (E4) into Eq. (D5), we plot the theoretical curves of the entanglement fidelity as a function of the generation probability for different distances, as shown in Fig. 8. The entanglement fidelity first increases and then decreases with increasing generation probability. When the generation probability is relatively low, multi-photon events are rare and have little impact on the fidelity of the entangled photon pairs; consequently, the entanglement fidelity increases monotonically with the generation probability. However, when the generation probability is relatively high, multi-photon events have a more pronounced impact on the fidelity, causing the entanglement fidelity to decrease monotonically as the generation probability increases. In addition, as the distance increases, the maximum entanglement fidelity decreases, while the generation probability required to achieve this maximum increases. This behavior mainly arises from the following reasons: First, the reduced transmittance of the quantum channel lowers the entanglement fidelity. Second, although an increased generation probability enhances the entanglement fidelity, it also introduces multi-photon noise, which further reduces the entanglement fidelity.

Resolving the trade-off between the generation probability and multi-photon noise of SPDC sources remains an important direction for future exploration. A near-ideal photon-number-resolving detector (PNR) can, in principle, completely eliminate the trade-off between fidelity and generation probability by post-selecting and discarding multi-pair events. [58,84] However, fabricating near-ideal PNR detectors is extremely difficult due to limitations such as the cryogenic operating environment, the trade-off between detection efficiency and dark counts, and the finite fidelity at high photon numbers. [85,86] Therefore, adopting a multiplexing architecture at low generation probability has become another important technical approach for balancing the generation probability of SPDC sources and the fidelity of entangled photon pairs. [59,87]

Acknowledgment

This work is supported by the National Natural Science Foundation of China (Grants No.12404407, No.12225405), Guangdong Provincial Quantum Science Strategic Initiative (GDZX2504005, GDZX2404001, GDZX2404003, GDZX2304002), and Guangdong Basic and Applied Basic Research Foundation (2026A1515030019).

References

[1] Kimble H J 2008 *Nature* **453** 1023
[2] Wehner S, Elkouss D, and Hanson R 2018 *Science* **362** eaam9288
[3] David A, Karl K B, Hannes B, et al. 2021 *PRX Quantum* **2** 017002
[4] Koji A, Sophia E E, David E, et al. 2023 *Rev. Mod. Phys.* **95** 045006
[5] Gottesman D and Chuang I L 1999 *Nature* **402** 390
[6] Duan L M, Blinov B B, Moehring D L, and Monroe C 2004 *Quantum Inf. Comput.* **4** 165
[7] Li Y and Benjamin S C 2012 *New J. Phys.* **14** 093008
[8] Cuomo D, Caleffi M, Cacciapuoti A S 2020 *IET Quantum Communication* **1** 3
[9] Wasilewski W, Jensen K, Krauter H, et al. 2010 *Phys. Rev. Lett.* **104** 133601
[10] Gottesman D, Jennewein T, and Croke S 2012 *Phys. Rev. Lett.* **109** 070503
[11] Komar P, Kessler E M, Bishof M, et al. 2014 *Nature Phys.* **10** 582
[12] Nichol B C, Srinivas R, Nadlinger D P, et al. 2022 *Nature* **609** 689
[13] Simon C 2017 *Nat. Photonics* **11** 678

[14] Meister J, Kleinpaß P, and Orsucci D 2025 *EPJ Quantum Technol.* **12** 5

[15] Liu P X, Lin Y P, Zhou Z Q, Li C F, and Guo G C 2026 *Phys. Rev. A* **113** 022614

[16] Dawar M, Paillet C, Vyas N, et al. 2026 *arXiv: 2603.11127v1 [quant-ph]*

[17] Liu J L, Luo X Y, Yu Y, et al. 2024 *Nature* **629** 579

[18] Yu Y, Ma F, Luo X Y, et al. 2020 *Nature* **578** 240

[19] van Leent T, Bock M, Fertig F, et al. 2022 *Nature* **607** 69

[20] Lu B W, Yang C W, Wang R Q, et al. 2026 *Science* **391** 592

[21] Krutyanskiy V, Galli M, Krcmarsky V, et al. 2023 *Phys. Rev. Lett.* **130** 050803

[22] Liu W Z, Zhou Y B, Chen J P, et al. 2026 *Nature* **652** 51

[23] Knaut C M, Suleymanzade A, Wei Y C, et al. 2024 *Nature* **629** 573

[24] Stolk A J, van der Enden K L, Slater M C, et al. 2024 *Sci. Adv.* **10** eadp6442

[25] Lago-Rivera D, Grandi S, Rakonjac J V, et al. 2021 *Nature* **594** 37

[26] Briegel H J, Dur W, Cirac J I, et al. 1998 *Phys. Rev. Lett.* **81** 5932

[27] Duan L, Lukin M, Cirac J, and Zoller P 2001 *Nature* **414** 413

[28] Chou C W, Laurat J, Deng H, et al. 2007 *Science* **316** 1316

[29] Yuan Z S, Chen Y A, Zhao B, et al. 2008 *Nature* **454** 1098

[30] Pu Y F, Zhang S, Wu Y K, et al. 2021 *Nat. Photonics* **15** 374

[31] Simon C, de Riedmatten H, Afzelius M, et al. 2007 *Phys. Rev. Lett.* **98** 190503

[32] Collins O A, Jenkins S D, Kuzmich A, et al. 2007 *Phys. Rev. Lett.* **98** 060502

[33] Munro W J, Harrison K A, Stephens A M, et al. 2010 *Nat. Photonics* **4** 792

[34] Zhang S, Shi J, Liang Y, et al. 2024 *Nat. Commun.* **15** 10306

[35] Wang M, Jiao H, Lu J, et al. 2024 *Laser Photonics Rev.* **18** 2300825

[36] Cui Z B, Wang Z Q, Lai P C, et al. 2025 *Nat. Commun.* **17** 697

[37] Brask J B and Sørensen A S 2008 *Phys. Rev. A* **78** 012350

[38] Tsujimoto Y, You C, Wakui K, et al. 2020 *New J. Phys.* **22** 023008

[39] Fang K and Goldschmidt E A 2025 *Phys. Rev. A* **111** 062618

[40] Childress L, Taylor J M, Sørensen A S, et al. 2006 *Phys. Rev. Lett.* **96** 070504

[41] Sangouard N, Dubessy R, and Simon C 2009 *Phys. Rev. A* **79** 042340

[42] Sangouard N, Simon C, de Riedmatten H, and Gisin N 2011 *Rev. Mod. Phys.* **83** 33

[43] Kim H, Kwon O, and Moon, H S 2019 *Sci. Rep.* **9** 5031

[44] Hajomer A A E, Derkach I, Usenko V C, et al. 2025 *Phys. Rev. Lett.* **135** 170804

[45] van Leent T, Bock M, Garthoff R, et al. 2020 *Phys. Rev. Lett.* **124** 010510

[46] Hu P, Li H, You L, et al. 2020 *Opt. Express* **28** 36884

[47] Cho Y W, Campbell G T, Everett J L, et al. 2016 *Optica* **3** 100

[48] Buser G, Mottola R, Cotting B, Wolters J, and Treutlein P 2022 *PRX Quantum* **3** 020349

[49] Körber M, Morin O, Langenfeld S, Neuzner A, Ritter S, and Rempe G 2018 *Nat. Photonics* **12** 18

[50] Hänni J, Rodríguez-Moldes A E, Appas F, et al. 2025 *Phys. Rev. X* **15** 041003

[51] Dong M X, Zhang W H, Zeng L, et al. 2023 *Phys. Rev. Lett.* **131** 240801

[52] Liu S, Wang Y, Saleem Y, et al. 2025 *Nature* **643** 1234

[53] Guo J, Wu Z, Bao G, et al. 2025 *Phys. Rev. Lett.* **135** 170802

[54] Patomaki S M, Sirotin M, Englund D R, et al. 2026 *Opt. Express* **34** 6561

[55] Petrovich M, Numkam Fokoua E, Chen Y, et al. 2025 *Nat. Photonics* **19** 1023

[56] Braunstein S L, Fuchs C A, Kimble H J, and van Loock P 2001 *Phys. Rev. A* **64** 022321

[57] Chahine Y K, Richardson J G, Katz E J, et al. 2026 *arXiv:2603.19489v1 [quant-ph]*

[58] Davis S I, Mueller A, Valivarthi R, et al. 2022 *Phys. Rev. Applied* **18** 064007

[59] Dhara P, Johnson S J, Gagatsos C N, et al. 2022 *Phys. Rev. Applied* **17** 034071

[60] Hahn F, Pappa A, and Eisen J 2019 *npj Quantum Inf.* **5** 76

[61] Li B, Goodenough K, Rozpedek F, and Jiang L 2025 *Phys. Rev. Lett.* **134** 190801

[62] Haldar S, Barge P J, Cheng X, et al. 2025 *Commun. Phys.* **8** 132

[63] Shao Y, Guha S, and Motter A E 2025 *Phys. Rev. Appl.* **24** 024033

[64] Vinet S, Tannous R, and Jennewein T 2025 *EPJ Quantum Technol.* **12** 8

[65] Shi X, Mohanraj S S, Dhyani V, et al. 2024 *Light Sci. Appl.* **13** 282

[66] Liu S, Wang Y, Saleem Y, et al. 2025 *Nature* **643** 1234

[67] Jiao X F, Zheng M Y, Chen Y H, et al. 2025 *Phys. Rev. Lett.* **135** 250803

[68] Meng R R, Liu P X, Liu X, et al. 2026 *Nat. Photonics* **20** 437

[69] Wang Y, Li J, Zhang S, et al. 2019 *Nat. Photonics* **13** 346

[70] Xu Y L, Zhang L, Zhang C, et al. 2025 *Phys. Rev. Lett.* **135** 230803

[71] Arenskoetter E, Bauer T, Kucera S, et al. 2023 *npj Quantum Inf.* **9** 34

[72] Yang Y, Wang B, Lin J C, et al. 2026 *arXiv: 2603.01745v1 [quant-ph]*

[73] Cohen M, Martin A, Dalidet R, et al. 2026 *APL Quantum* **3** 016101

[74] Hong H, Xiang X, Quan R, et al. 2026 *arXiv: 2602.19013v1 [quant-ph]*

[75] Bennett C H, Brassard G, Popescu S, et al. 1996 *Phys. Rev. Lett.* **76** 722

[76] Dür W, Briegel H J, Cirac J I, and Zoller P 1999 *Phys. Rev. A* **59** 169

[77] Gu H, Li Z, Yu R, et al. 2023 *arXiv:2301.08269v3 [quant-ph]*

[78] Magesan E, Gambetta J M, and Emerson J 2012 *Phys. Rev. A* **85** 042311

[79] Egorova E Y, Kazmina A S, Simakov I A, et al. 2025 *arXiv:2405.10886v2 [quant-ph]*

[80] Kazmina A S, Polyanskiy A M, Egorova E Y, et al. 2025 *arXiv:2506.20529v1 [quant-ph]*

[81] Wallnöfer J, Hahn F, Wiesner F, et al. 2024 *PRX Quantum* **5** 010351

[82] Tiedau J, Bartley T J, Harder G, et al. 2019 *Phys. Rev. A* **100** 041802

[83] Tubío V D, Dijksman M C, and Borregaard J 2026 *Quantum Sci. Technol.* **11** 035029

[84] Stasi L, Caspar P, Brydges T, et al. 2023 *Quantum Sci. Technol.* **8** 045006

[85] Schapeler T, Mischke T, Schlue F, et al. 2026 *APL Quantum* **3** 016102

[86] Ding C, Zhang X, Xiong J, et al. 2025 *ACS Photonics* **12** 4924

[87] Shapiro J H, Embleton C, Raymer M G, et al. 2025 *arXiv:2507.14427v4 [quant-ph]*